

The Destruction Of Laser-Induced Phase-Transition Nanoparticles Triggered By Low-Intensity Ultrasound: An Innovative Modality To Enhance The Immunological Treatment Of Ovarian Cancer Cells

This article was published in the following Dove Press journal:
International Journal of Nanomedicine

Wan Xie,^{1,2} Shen Yin Zhu,³
Biyong Yang,⁴ Chunyan Chen,¹
Shuning Chen,¹ Yujiao Liu,¹
Xuyuan Nie,⁵ Lan Hao,²
Zhigang Wang,²
Jiangchuan Sun,¹
Shufang Chang¹

¹Department of Obstetrics and Gynecology, The Second Affiliated Hospital of Chongqing Medical University, Chongqing 400010, People's Republic of China; ²Institute of Ultrasound Imaging, Second Affiliated Hospital of Chongqing Medical University, Chongqing 400010, People's Republic of China; ³Department of Pharmacy, The First Affiliated Hospital of Chongqing Medical University, Chongqing 400016, People's Republic of China; ⁴Chongqing Institute for Food and Drug Control, Chongqing 401121, People's Republic of China; ⁵School of Biological and Chemical Engineering, Chongqing University of Education, Chongqing 400067, People's Republic of China

Correspondence: Shufang Chang;
Jiangchuan Sun
Department of Obstetrics and Gynecology, The Second Affiliated Hospital of Chongqing Medical University, 74 Linjian Road, Yuzhong District, Chongqing 400010, People's Republic of China
Tel +86 023 6369 3279
Fax +86 023 6510 4238
Email shfch2018@hospital.cqmu.edu.cn; sunjiangchuan@126.com

Purpose: Photodynamic therapy (PDT), sonodynamic therapy (SDT), and oxaliplatin (OXP) can induce immunogenic cell death (ICD) following damage-associated molecular patterns (DAMPs) exposure or release and can be united via the use of nanoplateforms to deliver drugs that can impart anti-tumor effects. The aim of this study was to develop phase-transition nanoparticles (OI_NPs) loaded with perfluoropentane (PFP), indocyanine green (ICG), and oxaliplatin (OXP), to augment anti-tumor efficacy and the immunological effects of chemotherapy, photodynamic therapy and sonodynamic therapy (PSDT).

Methods: OI_NPs were fabricated by a double emulsion method and a range of physicochemical and dual-modal imaging features were characterized. Confocal microscopy and flow cytometry were used to determine the cellular uptake of OI_NPs by ID8 cells. The viability and apoptotic rate of ID8 cells were investigated using the 3-(4,5-dimethyl-2-thiazolyl)-2,5-diphenyl-2-H-tetrazolium bromide (MTT) assay and flow cytometry. Flow cytometry, Western blotting, and luminometric assays were then used to investigate the exposure or release of crucial DAMPs such as calreticulin (CRT), high mobility group box 1 (HMGB1), and adenosine-5'-triphosphate (ATP). Tumor rechallenge experiments were then used to investigate whether treated ID8 cells underwent ICD. Finally, cytotoxic T lymphocyte (CTL) activity was determined by a lactate dehydrogenase (LDH) assay.

Results: Spherical OI_NPs were able to carry OXP, ICG and PFP and were successfully internalized by ID8 cells. The application of OI_NPs significantly enhanced the phase shift ability of PFP and the optical characteristics of ICG, thus leading to a significant improvement in photoacoustic and ultrasonic imaging. When combined with near-infrared light and ultrasound, the application of OI_NPs led to improved anti-tumor effects on cancer cells, and significantly enhanced the expression of DAMPs, thus generating a long-term anti-tumor effect.

Conclusion: The application of OI_NPs, loaded with appropriate cargo, may represent a novel strategy with which to increase anti-tumor effects, enhance immunological potency, and improve dual-mode imaging.

Keywords: ovarian cancer, multifunctional nanoparticles, photo-sonodynamic therapy, immunogenic cell death, reactive oxygen species

Introduction

Ovarian malignancy is one of the most lethal gynecological cancers, is associated with a poor prognosis, and is often resistant to conventional therapies.¹ Therefore, it is vital to develop innovative therapeutic modalities for the administration of drug treatments to patients with advanced or recurrent ovarian cancer.

Immunotherapy harnesses the natural ability of the host immune system to distinguish, target, and eradicate tumor cells, thus providing a useful modality for the treatment of cancer.² Immunogenic cell death (ICD) triggers an anti-tumor immunological reaction in which dying tumor cells solicit an intense immune reaction, thus creating an “anticancer vaccine”.³ ICD is known to be induced by the emission or release of highly immunostimulatory signals that enhance the immunogenicity of damaged cells; these signals are referred to as damage associated molecular patterns (DAMPs).⁴ These specific molecules are now considered to represent useful biochemical markers of ICD, and include the secretion of high mobility group box 1 (HMGB1), the secretion of adenosine-5'-triphosphate (ATP), and the translocation of calreticulin (CRT) from the endoplasmic reticulum to the cell surface.³⁻⁵ These crucial DAMPs first attach to their own receptors, and then recruit and activate immunocytes.³⁻⁵ The translocation of CRT to the cell surface creates an “eat-me” signal that promotes professional phagocytic cells, such as dendritic cells (DCs), to engulf cancer cells due to the presentation of tumor antigens.^{6,7} HMGB1 serves as a proinflammatory signal and binds to toll-like receptor 4 (TLR4) on the surface of DCs, thus facilitating the presentation of tumor antigens to T cells.^{8,9} Extracellular ATP acts as a “find-me” signal that stimulates the swift aggregation of antigen-presenting cells in the periphery of dying cancer cells.^{10,11} Collectively, the endogenous danger signals that stem from the sufficient emission of DAMPs, cause an immunocompetent host to elicit the changes in their immunological system, thus creating an awareness to abnormal cancer cells, and the initiation of the host’s immune response.^{3,12} A growing body of evidence now indicates that oxaliplatin (OXP), a conventional chemotherapeutic, can induce ICD to regulate the immune system and elicit an immunoreaction that maintains a long-term durable therapeutic effect.¹³⁻¹⁵

Over recent years, it has become increasingly common to develop nanoscale perfluorocarbon (PFC) droplets as novel multi-mode imaging contrast agents and drug delivery systems.¹⁶⁻¹⁸ PFC droplets exhibit negligible absorption properties in the near-infrared (NIR) region.^{19,20} Consequently, optical absorption agents must be entrapped into the droplets in order to achieve a sufficient level of energy absorption.¹⁹ When excited by visible light of an appropriate wavelength, these modified droplets experience an increase in temperature, thus causing the liquid droplet to vaporize and create a bubble phase that is useful

for ultrasound (US) imaging and photoacoustic (PA) signals.¹⁸ During this progress, a complicated photochemical reaction occurs that produces cytotoxic reactive oxygen species (ROS), generally in the form of singlet oxygen ($^1\text{O}_2$). This process is known as photodynamic therapy (PDT) and is an efficient method for killing cells.^{21,22}

A number of studies have demonstrated that PDT-treated cancer cells can cause ICD *in vitro*.²³⁻²⁵ Vaccination with cancer cells that had been pre-treated with PDT *in vitro* has been shown to restrict the growth of tumors in cells of the same origin.²³ However, light is only able to penetrate to a certain depth, thus limiting the use of this technique to superficial lesions.²⁶ Unlike PDT, sonodynamic therapy (SDT) can focus ultrasound (US) energy to target much deeper regions of tissue and activate the local cytotoxicity of the sonosensitizer when accumulated at the site of cancer.^{27,28} Although the differences between PDT and SDT have not been fully elucidated, both methods appear to generate cytotoxic effects by generating ROS, thus inducing cell apoptosis and necrosis.²⁹⁻³¹ Recent studies have shown that SDT can induce ICD.³² Moreover, the combined application of PDT and SDT (PSDT) may help us to reduce the doses of both ultrasound/light energy and sensitizer, thus attenuating potential side effects and providing a more robust form of anticancer therapy than any monotherapy.^{29,30,33} The ability of indocyanine green (ICG) to exhibit fluorescent properties in the NIR spectrum has been extensively employed in PDT.³⁴ Recent studies have found that photosensitive ICG can also be excited by ultrasound.³⁵

Previously, we described the synthesis of an efficient delivery vehicle for photo/sonosensitizers, and/or chemotherapeutic drugs, to treat ovarian cancer cells, or MH7A cells, with remarkable therapeutic effects.^{36,37} In the present study, we fabricated a novel type of nanoparticle by utilizing poly(lactide-*co*-glycolic acid) (PLGA) which was then used to enhance the delivery system we described previously. The system described herein combined safe materials with drugs to construct multifunctional phase-transition nanoparticles OI_NPs loaded with perfluoropentane (PFP), indocyanine green (ICG), and oxaliplatin (OXP). These nanostructures provided us with tools that possessed diagnostic imaging contrast capability, combined with the therapeutic and immune-potent actions of photo/sonodynamic and other drugs to kill cancer and enhance anti-tumor efficacy.

Materials And Methods

Cell Lines And Animals

ID8 cells (syngeneic to C57BL/6 mice) were generously provided by Dr. Katherine Roby (University of Kansas Medical Center, USA) and Dr. Yi Li (Gynecology Oncology Center of Peking University People's Hospital, China). ID8 cells were cultured in DMEM (Gibco, NY, USA) containing 5% fetal bovine serum, 1% streptomycin, and 1% penicillin, at 37°C under 5% CO₂. The use of the ID8 cell line was approved by the Ethics Committee of the Second Affiliated Hospital of Chongqing Medical University. Female C57BL/6 mice, aged 6–8 weeks, were obtained from the Laboratory Animal Center of Chongqing Medical University and maintained under specific-pathogen-free conditions. All procedures related to animal experiments were approved by the Ethics Committee of the Second Affiliated Hospital of Chongqing Medical University.

Preparation And Characterization Of NPs

PLGA (Medical Polymer Materials, Shangdong, PR China) nanoparticles, loaded with PFP (Strem Chemicals, Newburyport, MA, USA), OXP (MedChemExpress, NJ, USA) and ICG (Aladdin, Shanghai, PR China), which we referred to as OI_NPs, were prepared as described in our previous publications.^{36,37} In brief, an ultrasonic probe (Sonics & Materials, Inc, Fairfield, CT) was used to sonicate 6mg/mL of an aqueous solution of OXP, and 200µl of PFP for 30s. Next, the mixture was added to 2ml of methylene chloride (containing 2mg of ICG and 50mg of PLGA) and sonicated using the ultrasonic probe. The resultant emulsion was then poured into a solution of 4% polyvinyl alcohol (Sigma-Aldrich, St Louis, MO, USA) and emulsified by sonication. The emulsion was then stirred for 4h to evaporate methylene chloride. The solution of OI_NPs was then centrifuged at 12,000 rpm for 5 min at 4°C (Biofuge Stratos Centrifuge; Thermo Fisher Scientific, Germany) prior to the removal of the supernatant. The precipitate was then washed in water and re-centrifuged. The washed precipitate was then resuspended in water and stored at 4°C to await further experimentation. Blank NPs, without ICG and OXP, and I_NPs without OXP, were also prepared in a similar manner. All steps were performed at low temperature and in the dark. Transmission electron microscopy (TEM, FEI Tecnai G2 F20, FEI Company, USA), and scanning electron microscopy (SEM, FEI Inspect F50, FEI Company, USA), were

used to investigate the morphology and structure of the newly synthesized OI_NPs. The diameter, polydispersity index (PDI), and surface potential, of different NPs were determined by dynamic light scattering (DLS) (Zetasizer Nano ZS, Malvern Instruments, Malvern, UK). The entrapment efficiency and loading of ICG was evaluated by an ultraviolet-visible (UV-Vis) spectrophotometer (260-Bio, Thermo Fisher Scientific). We measured the absorbance of unencapsulated ICG in supernatant at a wavelength of 780 nm to determine its concentration, and then calculated the entrapment and loading efficiency of encapsulated ICG. Following centrifugation, high performance liquid chromatography (HPLC) was performed to analyze the OXP present in the supernatant. Drug entrapment efficiency, and loading, were calculated according to the following formulas: entrapment efficiency (%) = $([\text{drug added into formulation} - \text{drug in supernatant}] / \text{drug added into formulation}) \times 100\%$; loading (% w/w) = $([\text{drug added into formulation} - \text{drug in supernatant}] / \text{total mass of NPs}) \times 100\%$. Absorption spectra were determined by a UV-Vis spectrophotometer (scanning wavelength ranged from 550 to 850 nm). The emission spectra of each sample were detected using a fluorescence spectrometer (Cray Eclipse, Agilent Technologies) and recorded from 770 to 860 nm with excitation at 760 nm. The absorbance (at 780 nm), and the fluorescence intensity (at maximal emission wavelength), were detected at three days intervals to evaluate optical stability.

US And PA Imaging: In Vitro Gel Experiments

The capacity of OI_NPs to act as contrast agents for dual-modal imaging was evaluated by an agar-gel model (2% agar w/v in de-aerated water). A pipette tip was inserted into the gel to create a void. PBS, free ICG, or NP solutions, were then placed into the void and irradiated with a laser (808nm diode laser, Mid-River Ltd, Xi'an, China) at 1.5W/cm² for 2 min. During the time that each agent was exposed to irradiation, we captured contrast-enhanced ultrasound (CEUS), and B-mode images, via an ultrasonic diagnostic instrument (MyLab 90; Esaote, Genoa, Italy). Then, we used DFY (invented by the Institution of Ultrasound Imaging of Chongqing Medical University) to measure the Echo Intensity (EI) in B-mode and contrast mode separately. PA-mode signals of the samples were also obtained and analyzed using the VEVO LASR PA imaging system

(VIVO 2100, FUJIFILM Visual Sonic, Inc, USA), as described above.

Determination Of Cellular Uptake

Next, ID8 cells were seeded (at a density of 1×10^6 ID8 cells per well) onto six-well plates and cultured overnight. On the second day, the original media was replaced by culture media, or culture media containing OI_NPs labeled with Dil dye (containing ICG $8.5 \mu\text{g/mL}$, OXP $6.0 \mu\text{g/mL}$) for 6 h co-incubation. Subsequently, the cells were washed in sterile PBS and fixed with 4% paraformaldehyde (PFA) for 15 min. 2-(4-Amidinophenyl)-6-indolecarbamidine dihydrochloride (DAPI) was then applied to stain cell nuclei. Finally, we evaluated cellular uptake ability by confocal laser scanning microscopy (CLSM, Leica TCS SP8, Heidelberg, Germany). In addition, ID8 cells were co-incubated, harvested and measured by flow cytometry without fixation in 4% PFA fixed and DAPI staining. This allowed us to calculate the mean fluorescence intensity.

The Cytotoxicity Of OI_NPs In ID8 Cells

ID8 cells were seeded into 48-well plates and co-incubated with OI_NPs at various OXP concentrations. After 6h of co-incubation, ID8 cells were washed with PBS and the media in each well was replaced with fresh media. Next, the OI_NPs group was irradiated with 1.5 W/cm^2 of light at a wavelength of 808nm for 2min, and then exposed to 1.0 W/cm^2 of low-intensity ultrasound for 1min in the dark. After 24h of treatment, we used the 3-(4,5-Dimethylthiazol-2-yl)-2,5-diphenyltetrazolium bromide (MTT) assay to determine cell viability. Next, ID8 cells were seeded and cultured for a 24h period. The cell-culture media was then replaced by complete media containing equivalent concentrations of free OXP, I_NPs, or OI_NPs (concentration of ICG, $8.5 \mu\text{g/mL}$; concentration of OXP, $6.0 \mu\text{g/mL}$). The rest of the procedure was the same as that described above.

The Use Of Flow Cytometry To Analyze Apoptosis

Next, 1×10^6 cancer cells were seeded into each well of a six-well plate and were cultured overnight. The next day, the cells were washed in PBS and the culture media was changed to a complete medium containing equal concentrations of free OXP, I_NPs, and OI_NPs (ICG concentration, $8.5 \mu\text{g/mL}$; OXP concentration, $6.0 \mu\text{g/mL}$) for 6 h of co-incubation. The cells were then washed in PBS and new culture media added. According to different experimental groupings, the

cells were irradiated with 1.5 W/cm^2 of light at a wavelength of 808nm for 2min, and exposed to 1.0 W/cm^2 of low-intensity ultrasound for 1 min in the dark. Twenty-four hours later, the rate of apoptosis in the ID8 cells was evaluated by Annexin V/Propidium iodide (PI) double staining and quantified by flow cytometry.

Flow Cytometry For CRT

For flow cytometry analysis, the ID8 cells were co-incubated with different drug formulations (free OXP, I_NPs, and OI_NPs) for 6 h. After three washes in PBS, the cells were irradiated in several different ways according to experimental grouping (with or without a laser for 2 min and ultrasound for 1min). After 4 h of treatment, the cells were washed twice with cold PBS and fixed in 0.25% PFA for 5 min. Then, the cells were stained with rabbit anti-calreticulin antibody (Abcam, Cambridge, UK) in cold blocking buffer (2% FBS in PBS) for 40min at 4°C without permeabilization. Next, the cells were incubated with an Alexa Fluor 488-conjugated polyclonal secondary antibody (Abcam, Cambridge, UK) diluted in blocking buffer for 30 min at 4°C in the dark, and then stained with PI for 5 min. Samples were then analyzed by flow cytometry to quantify CRT expression on the cell surface; CRT-positive cells were gated on PI-negative cells.

HMGB1 Release Assay And The Quantification Of Extracellular ATP

After 24h exposure to different treatments, the supernatant and cells were collected separately. We then used Western blotting to detect the release of HMGB1 into the cell culture supernatant and its translocation to the cytoplasm. BSA and β -actin were used as loading controls. A Luminometric ATP Assay Kit (AAT Bioquest, CA, USA) was then utilized to quantify the secretion of ATP into the supernatant. Mix ATP monitoring enzyme, ATP sensor, and reaction buffer to prepare ATP assay solution in accordance with the manufacturer's instructions. Following exposure to different treatments, the samples were mixed with the ATP assay solution to detect the intensity of luminescence. The concentration of ATP was calculated in accordance with a standard calibration curve generated using a standard ATP solution.

Measurement Of ROS

2',7'-dichlorofluorescein diacetate (DCFH-DA) was used as an indicator of fluorescence to detect the generation of intracellular ROS. In brief, 1×10^6 ID8 cells were seeded

into each well of a 6-well plate. Following overnight incubation, the culture medium was replaced with fresh medium containing free OXP, I_NPs, or OI_NPs (8.5µg/mL of ICG; 6.0µg/mL of OXP) and then co-incubated with the ID8 cells for 6 h. Subsequently, cells were washed three times in PBS. DCFH-DA (10 µM) was then diluted into serum free medium and co-incubated with cells for 30 min in the dark. Then, the cells were promptly irradiated with a 1.5 W/cm² laser for 2min and 1.0 W/cm² low-intensity ultrasound for 1min. Fluorescent signals were then detected by fluorescence microscopy and were quantified using a fluorescence microplate reader in accordance with the manufacturer's instructions.

Tumor Vaccination

ID8 cells were treated with equivalent concentrations of free OXP, I_NPs, or OI_NPs (8.5µg/mL of ICG, 6.0µg/mL of OXP) in vitro. Cells were then irradiated with a 1.5W/cm² laser for 2min and 1.0W/cm² ultrasound for 1min, in accordance with experimental grouping. Female C57BL/6 mice, 6–8 weeks old, were then inoculated with 3×10⁶ ID8 cells, which had been pre-treated in different ways (either Control or PSDT, I_NPs+PSDT, free OXP, OI_NPs, or OI_NPs+PSDT) via a subcutaneous route below the left shoulder. Seven days later, these mice were rechallenged by injecting 1×10⁶ live ID8 cells below the right shoulder. Tumor development was then monitored below the right shoulder; mice were defined as being tumor-free when palpation failed to detect the presence of tumorigenesis. After sixty days, animals bearing tumors were sacrificed. All mice were maintained under specific pathogen-free conditions and received care in accordance with the guidelines for the Care and Use of Laboratory Animals.

The Cytotoxic Response Of T Lymphocytes To Tumor Cells

Ten days after vaccination, the mice were sacrificed, and single spleen cell suspensions were generated, as described previously.³⁸ Splenocytes were used as effector cells, while ID8 cells were used as target cells. The CTL assay by lactate dehydrogenase (LDH) was carried out at an effector: target (E: T) ratio of 25:1, 50:1, and 100:1, over 4 hrs of co-incubation. LDH release was assessed according to the instructions provided with the lactate cytotoxicity assay kit (Beyotime Co, Shanghai, PR China).

Statistical Analysis

Data analysis was performed using GraphPad Prism (version 6.0) and all values are shown as mean ± standard deviation (SD). Data were analyzed by analysis of variance (ANOVA) with Dunnett's test, the unpaired Student's *t*-test, or the paired Student's *t*-test. Kaplan-Meier survival curves showed the time line for tumor development and were analyzed by the Gehan-Breslow-Wilcoxon test. A *P*-value < 0.05 indicated statistical significance.

Results

Preparation And Characterization Of OI_NPs

Spherical OI_NPs were successfully created with PLGA carrying PFP, OXP and ICG. Table 1 shows the physicochemical properties of types of NPs. There was no statistical difference among the size, PDI and zeta potential of three NPs. There was no statistical significance between the encapsulation efficiency and the loading of ICG in the I_NPs or OI_NPs. The loading of OI_NPs with OXP was 1.42±0.04%, as determined by the specific absorption spectra by HPLC. A schematic illustration of the OI_NPs is given in Figure 1A. The OI_NPs exhibited a spherical shell structure, as

Table 1 The Physicochemical Properties Of Nanoparticles Used In This Study

Groups	Size (nm)	PDI	Zeta Potential (mV)	Encapsulation Efficiency Of ICG(%)	ICG Loading (%)	Encapsulation Efficiency of OXP(%)	OXP Loading (%)
Blank NPs	258.60±15.19	0.12±0.07	-15.30±1.06	–	–	–	–
I_NPs	266.13±12.35	0.12±0.04	-14.73±0.68	56.09±3.89	2.16±0.15	–	–
OI_NPs	264.50±11.53	0.14±0.05	-15.50±2.78	55.90±2.45	2.03±0.09	26.02±0.72	1.42±0.04

Notes: Data are shown as mean ± SD (n=3). There was no statistical difference among three groups. No statistical significance between the encapsulation efficiency and the loading of ICG in the I_NPs or OI_NPs. The loading of OI_NPs with OXP was 1.42±0.04%, as determined by the specific absorption spectra by HPLC.

Abbreviations: PDI, polydispersity; ICG, indocyanine green; OXP, oxaliplatin; NPs, nanoparticles; PFP, perfluoropentane; I_NPs, ICG and PFP loaded NPs; OI_NPs, ICG, PFP and OXP loaded NPs; SD: standard deviation.

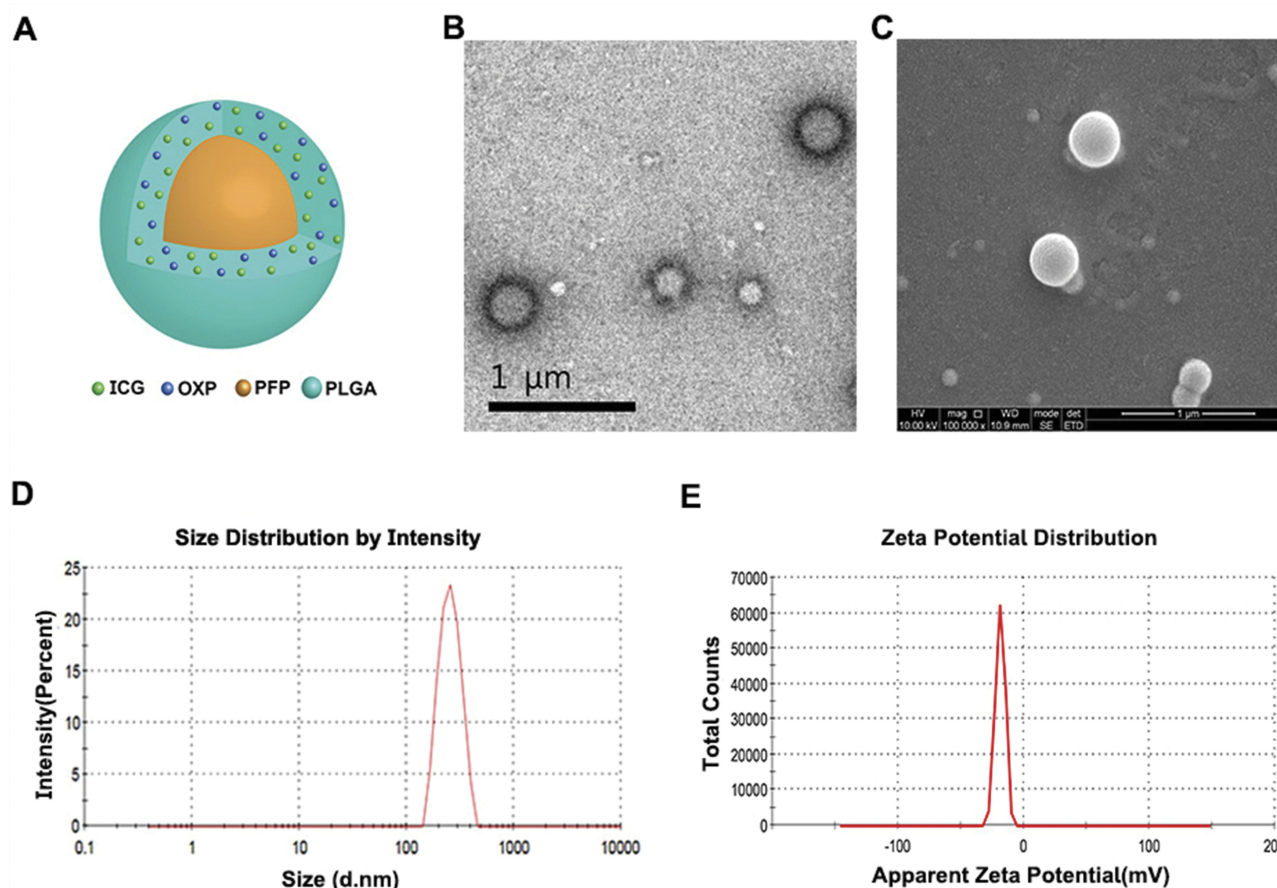


Figure 1 The morphology, structure, and characterization, of OI_NPs. **(A)** Schematic illustration of the structure of OI_NPs. **(B)** TEM image of OI_NPs. Scale bar represents 1 μm . **(C)** SEM image showing that OI_NPs possessed a smooth surface. Scale bar represents 1 μm . **(D)** The size distribution of OI_NPs, as measured by DLS. **(E)** The zeta potential of OI_NPs, as determined by DLS measurement.

Abbreviations: ICG, indocyanine green; OXP, oxaliplatin; PFP, perfluoropentane; PLGA, poly (DL-lactide-co-glycolic acid); OI_NPs, ICG, PFP and OXP loaded PLGA nanoparticles; TEM, transmission electron microscope; SEM, scanning electron microscopy, DLS, dynamic light scattering.

determined by TEM (Figure 1B). SEM imaging also showed that the OI_NPs had a spherical structure with a smooth surface (Figure 1C). According to DLS measurements, the spherical OI_NPs exhibited a Z-average diameter of 264.50 ± 11.53 nm with good symmetry (Figure 1D). The zeta potential of the OI_NPs was -15.50 ± 2.78 mV (Figure 1E). The optical properties, and stability, of the OI_NPs were also detected and are shown in Figure 2. The absorption peak of ICG loaded in PLGA(OI_NPs) was red-shifted by approximately 16 nm when compared with free ICG (Figure 2A). Measurement of the fluorescence spectra showed that the emission peak of ICG, when loaded in OI_NPs, was red-shifted by approximately 4 nm when compared with free ICG (Figure 2C). The emission spectra and absorbance of OI_NPs, and free ICG, were measured every three days to determine whether the ICG loaded into PLGA NPs was more stable than free ICG. Over 15 days of observation, free ICG showed a sharp reduction in stability when compared with

OI_NPs (Figure 2B and D). On the last day of observation, OI_NPs showed a reduction in absorption intensity by approximately 23%. However, the stability of free ICG had decreased dramatically by 67% (Figure 2B). The fluorescence intensity of OI_NPs had reduced to approximately 44% while that of free ICG had declined by almost 79% (Figure 2D). These results showed that PLGA nanoparticles represented a biocompatible and biodegradable carrier platform with improved ICG absorption and fluorescence stability, thus facilitating long-term storage.

Dual-Mode Imaging In Vitro Gel Experiments

Next, we investigated the probability of OI_NPs loaded with ICG and PFP to synthesize a multifunctional and biocompatible contrast agent for future goals of image-guided therapy. US imaging (Figure 3A) showed that there was no US enhancement in PBS and free ICG groups in contrast-

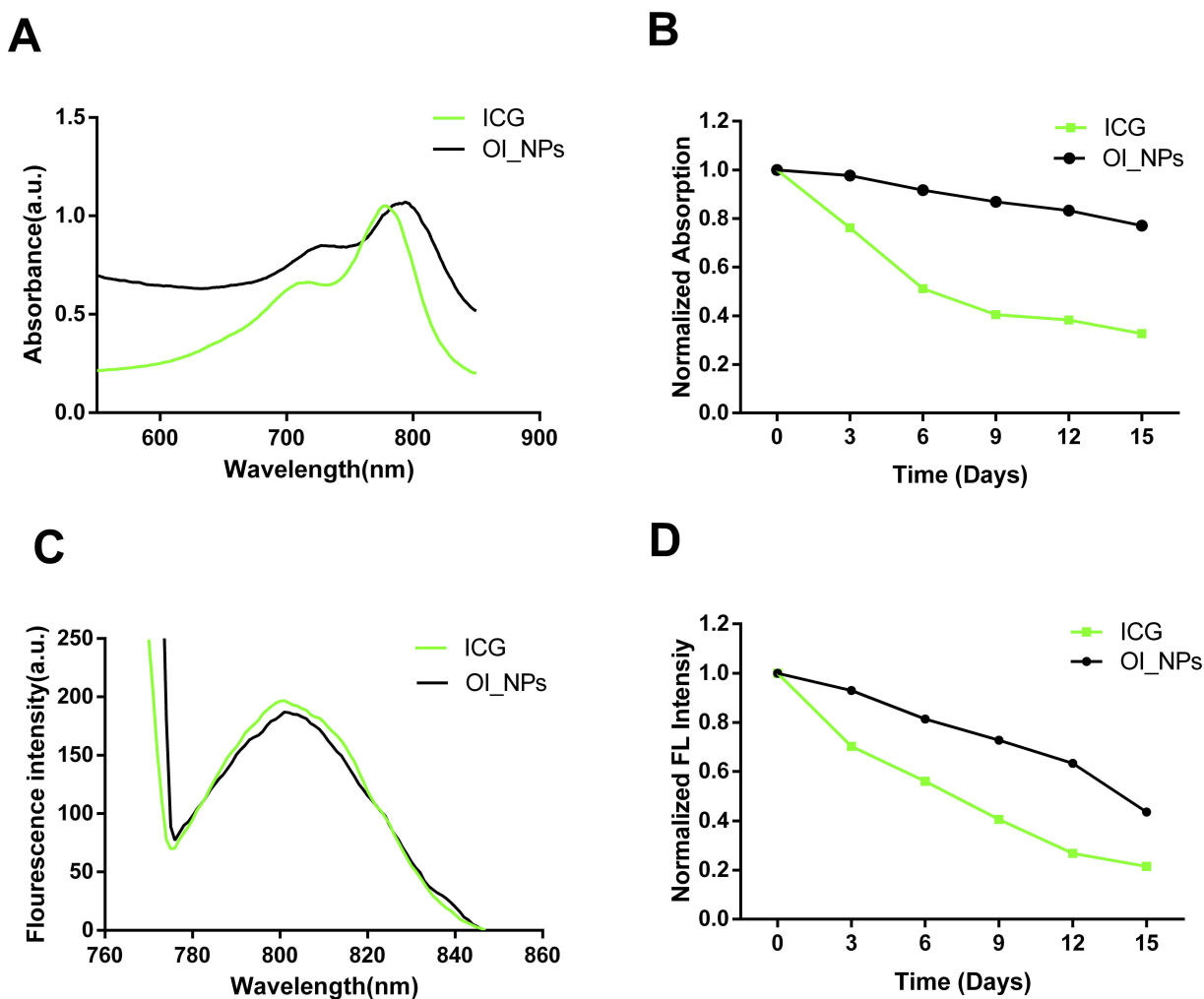


Figure 2 Measurement of the optical properties and stability of OI_NPs. **(A)** Absorption and **(C)** fluorescence spectra of free ICG and OI_NPs. **(B)** The absorbance stability and **(D)** fluorescence stability of free ICG and OI_NPs at 3-day intervals. These results demonstrated that OI_NPs had a higher stability than freely dissolved ICG. **Abbreviations:** ICG, indocyanine green; OI_NPs, indocyanine green, perfluoropentane and oxaliplatin loaded nanoparticles.

enhanced ultrasound (CEUS) mode, and B-mode, following laser illumination. Furthermore, minimal enhancement of US was observed in Blank NPs following laser irradiation for 2 min. The Blank NPs were PFP-loaded nanoparticles without ICG and OXP. This pattern of growth may be related to fact that the temperature of the PFP-loaded Blank NPs increased slightly after 808nm irradiation; this heat may have caused a small amount of PFP to undergo a phase change. The Echo Intensity (EI) of the OI_NPs group increased significantly, in both B-mode and CEUS mode (Figure 3B and C). This indicated that the OI_NPs were able to change phase in response to NIR irradiation and therefore have the potential to be used as a contrast-enhanced agent for US imaging.

PA signals were negligible for both the PBS and Blank NPs groups (Figure 3). Compared with other groups, the PA signal of the OI_NPs was significantly enhanced after

irradiation ($P < 0.05$). This may have been due to the optical absorption of ICG and the subsequent photothermal expansion resulting from the vaporization of PFP. The PA signal intensity decreased significantly in the free ICG group; presumably this was because ICG could be quenched easily when the ICG was not loaded onto the PLGA. These findings were in line with our semi-quantitative results (Figure 3E and F). Due to the improved ICG optical stability arising from PLGA encapsulation, together with the phase-transition ability of PFP, the OI_NPs represented a dual-model contrast agent for PA and US imaging.

In Vitro Cellular Uptake

CLSM and flow cytometry were used to investigate the ability of ID8 cells to absorb OI_NPs. These analyses clearly showed

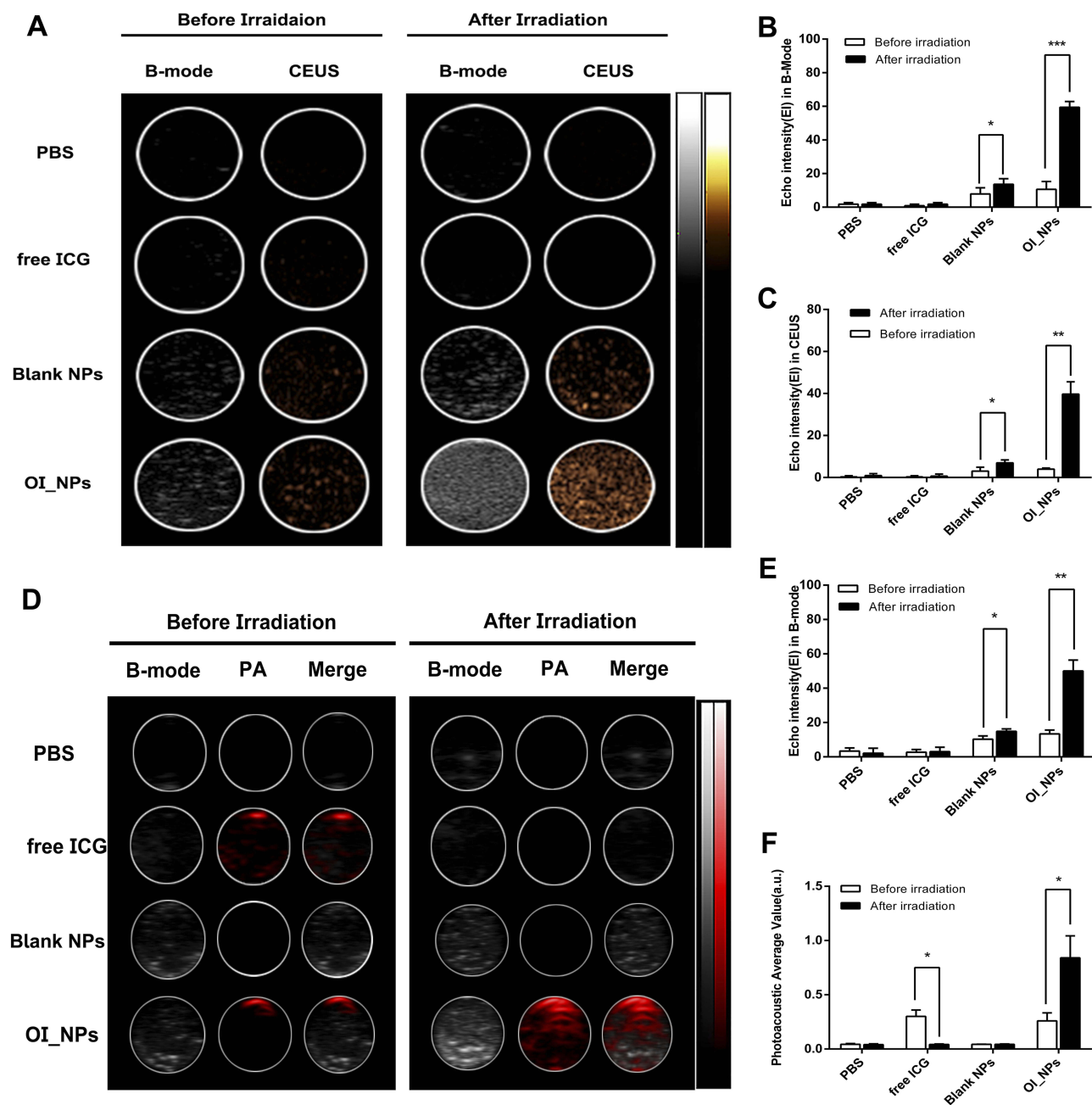


Figure 3 In vitro ultrasound and photoacoustic imaging of OI_NPs. (A) B-mode and CEUS imaging of different groups before and after irradiation in a phantom gel model. (B) and (C) EI in B-mode and CEUS mode after different treatments. (D) B-Mode and PA -Mode imaging of different groups before and after irradiation. (E) EI in B-Mode and (F) Mean PA. All values represent means \pm SD (n=3). The Student's paired t-test was used to compare data before irradiation and after irradiation. Levels of significance are indicated as * P <0.05; ** P <0.01; *** P <0.001.

Abbreviations: NPs, nanoparticles; ICG, indocyanine green; OI_NPs, indocyanine green, perfluoropentane and oxaliplatin loaded nanoparticles; CEUS, contrast-enhanced ultrasound; EI, echo intensity; US, ultrasound; PA, photoacoustic; SD, standard deviation.

that ID8 cells contained OI_NPs following co-incubation and that the OI_NPs were visible as an abundance of intracellular fluorescence signals surrounding the DAPI-stained ID8 nuclei (Figure 4A). Flow cytometry (Figure 4B and C) showed that when compared with the control group, the OI_NPs group had

a significantly higher mean fluorescence intensity (P <0.001). These results indicate that OI_NPs were able to be internalized by ID8 cells. Since OI_NPs can be taken up by cells in a highly efficient manner implies that these nanostructures may be beneficial for cancer therapy.

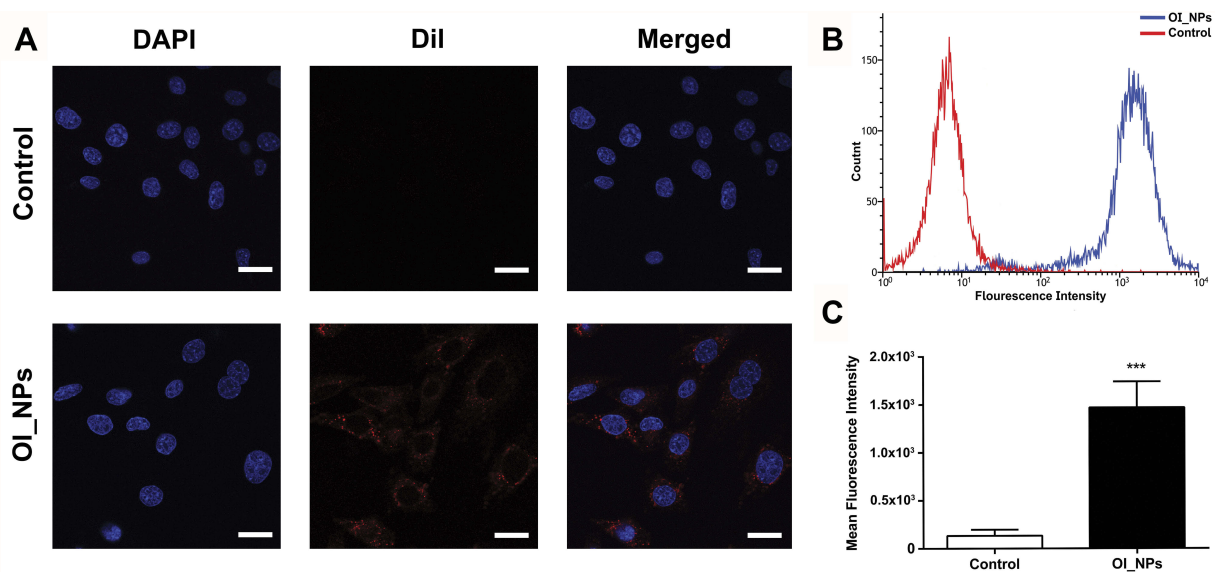


Figure 4 Cellular uptake of OI_NPs by ID8 cells. **(A)** CLSM images of the subcellular localization of ID8 cells. DAPI (blue) indicates nuclei while Dil (red) indicates OI_NPs. Scale bar represents 25 μm . **(B-C)** Flow cytometric analysis of mean fluorescence intensity in ID8 cells incubated with media (red) or OI_NPs (blue), for 6 h. Data are shown as means \pm SD ($n=3$). *** $P<0.001$ versus OI_NPs group.

Abbreviations: DAPI, 2-(4-amidinophenyl)-6-indolecarbamidine dihydrochloride; Dil, 1,1'-dioctadecyl-3,3,3',3'-tetramethylindocarbocyanine perchlorate; ICG, indocyanine green; OI_NPs, indocyanine green, perfluoropentane and oxaliplatin loaded nanoparticles; CLSM, confocal laser scanning microscopy; SD, standard deviation.

Cytotoxic Effects In Vitro

Next, we investigated the viability of ID8 cells with an MTT assay. ID8 cells were treated with various concentrations of OXP and showed a dose-dependent inhibitory effect on cell viability (Figure 5A). Furthermore, the same OXP concentration loaded in OI_NPs could inhibit more cell activity. Cell viability was particularly reduced when treated with OI_NPs +PSDT. The concentration of OI_NPs (8.5 $\mu\text{g}/\text{mL}$ of ICG and

6.0 $\mu\text{g}/\text{mL}$ of OXP) was then used in subsequent experiments to analyze the capacity of this combination therapy to induce ICD. This concentration of OI_NPs combined with PSDT caused more than 50% of the ID8 cells to die within 24 hrs. The cytotoxic effects of different treatments on ID8 cells is shown in Figure 5B. There was no significant cytotoxicity in the Control, PSDT, or I_NPs groups. The cell viability of the free OXP and OI_NPs groups was 80.94 \pm 1.04% and 75.72 \pm 5.44%, respectively. There were no significant differences in terms of cell viability between these two particular groups. OI_NPs combined PSDT induce stronger cell cytotoxicity than other groups ($P<0.001$). These results indicated that OI_NPs have significant potential as drug delivery vehicles because they show excellent synergy between the chemotherapeutic effects of OXP and the photo-chemical/sonochemical reactions of ICG.

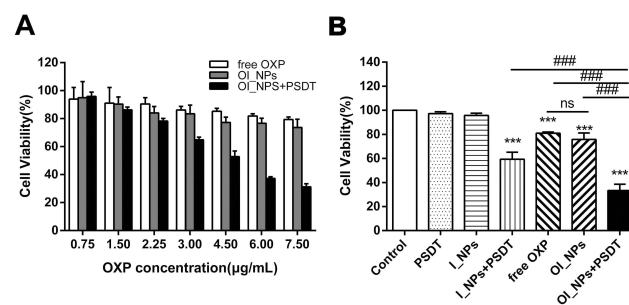


Figure 5 Detection of the viability of ID8 cells by MTT assay. **(A)** Cytotoxicity of different OXP concentrations, with different formulations, on ID8 cells, as determined by MTT assay. **(B)** Cell viability of ID8 cells under different treatments, as determined by the MTT assay (6.0 $\mu\text{g}/\text{mL}$ of OXP and 8.5 $\mu\text{g}/\text{mL}$ of ICG). Data in **(A)** and **(B)** represent the means \pm SD of three experiments. Data were analyzed using Student's *t*-tests and ANOVA. *** $P<0.001$ versus control group. #### $P<0.001$ between groups.

Abbreviations: MTT, 3-(4,5-dimethyl-2-thiazolyl)-2,5-diphenyl-2-H-tetrazolium bromide; ICG, indocyanine green; OXP, oxaliplatin; PFP, perfluoropentane; I_NPs, ICG and PFP loaded nanoparticles; OI_NPs, ICG, PFP and OXP loaded nanoparticles; PSDT, photo-sonodynamic therapy; SD, standard deviation; ns, no significant difference.

ICD Induced By OI_NPs Via The Mediation Of PSDT

Cancer cells undergoing ICD exhibit superior immunogenic potential when DAMPs release which are used as robust danger signals to trigger an immune response, including the translocation of CRT to the cell surface, the release of HMGB1, and the secretion of ATP, during cell death.³

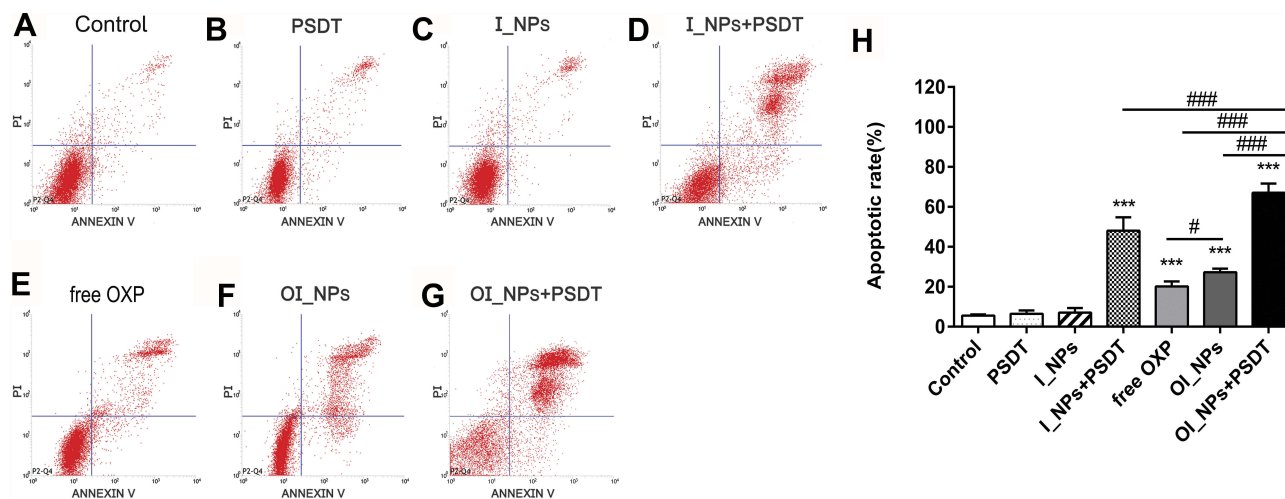


Figure 6 Apoptosis in ID8 cells, as detected by flow cytometry 24 h after different treatments. (A) Control; (B) PSDT; (C) I_NPs; (D) I_NPs + PSDT; (E) free OXP (F) OI_NPs; (G) OI_NPs+PSDT. (H) Statistical results of triplicate experiments. Results are presented as means \pm SD. Data were analyzed by the Student's *t*-test and ANOVA. Levels of significance are indicated as *** P <0.001 versus control group. # P <0.05 and ### P <0.001 between groups.

Abbreviations: ICG, indocyanine green; OXP, oxaliplatin; PFP, perfluoropentane; I_NPs, ICG and PFP loaded nanoparticles; OI_NPs, ICG, PFP and OXP loaded nanoparticles; PSDT, photo-sonodynamic therapy; SD, standard deviation.

We investigated the rate of apoptosis in ID8 cells in response to different treatments via the use of flow cytometry (Figure 6). The apoptotic trend in each treatment group was in accordance with data arising from the MTT assay when investigating cell viability. No obvious apoptosis was observed in the Control, PSDT, or I_NPs groups (Figure 6A–C; $5.51 \pm 0.68\%$, $6.47 \pm 1.69\%$, and $7.10 \pm 2.26\%$, respectively). However, there were significant differences in the rate of apoptosis when compared between the free OXP group ($20.15 \pm 2.49\%$) and the OI_NPs group ($27.20 \pm 1.82\%$) (P <0.05) (Figure 6E, F and H). The treatment of cells with OI_NPs induced a significantly higher rate of apoptosis than its free compound counterpart. When cells were treated with I_NPs, and exposed to laser and ultrasound, we detected a notable rate of apoptosis ($48.09 \pm 6.70\%$) (Figure 6D). The apoptotic rate of cells treated with OI_NPs + PSDT was significantly higher ($67.01 \pm 4.60\%$) than any of the other groups (P <0.001) (Figure 6G and H).

In order to investigate the ability of different treatments to induce CRT, we investigated the translocation of CRT in cells under different treatment regimens by flow cytometry (Figure 7A). A statistically significant increase of CRT was detected on the surface of cells treated with free OXP, OI_NPs, I_NPs +PSDT, and OI_NPs +PSDT. I_NPs only induced CRT translocation upon laser irradiation and ultrasound exposure, indicating that PSDT, but not ICG, elicits ICD. The most significant translocation of CRT occurred in cells treated with OI_NPs and exposed to laser and ultrasound. The translocation of CRT to the surface of ID8 cells was significantly more

extensive in cells treated OI_NPs than free OXP (P <0.05). Analysis of ATP secretion showed that compared with control, treatment with free OXP, OI_NPs, I_NPs+PSDT, and OI_NPs +PSDT, induced the secretion of more ATP (Figure 7B). Treatment with OI_NPs+PSDT showed the highest and most significant increase in ATP secretion when compared with the other treatments (P <0.001). As shown in Figure 7B, OI_NPs elicited a significantly higher rate of ATP secretion than free OXP in ID8 cells (P <0.01). These results show that PLGA NPs encapsulation enhances the ability of OXP to elicit the release of DAMPs and that in combination with PSDT leads to a further significant increase in the release of DAMPs. Western blotting

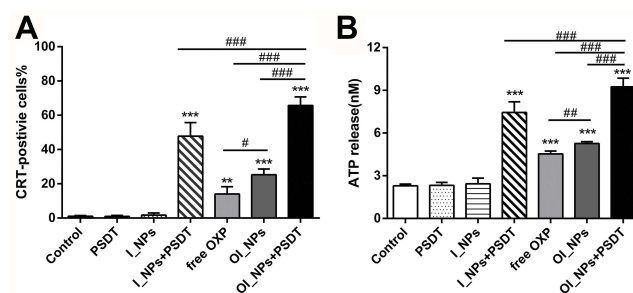


Figure 7 The ability of different treatments to induce CRT exposure and ATP secretion. (A) CRT exposure on the cell surface of ID8 cells was assessed by flow cytometry after different treatments. (B) The amount of released ATP was determined by a Luminometric ATP Assay Kit. Experiments were carried out in triplicate, and the results are presented as means \pm SD. Statistical analysis was performed using the Student's *t*-test and ANOVA. ** P < 0.01 and *** P <0.001 versus control group. # P <0.05, ### P <0.01 and #### P <0.001 between groups.

Abbreviations: CRT, calreticulin; ATP, adenosine-5'-triphosphate; ICG, indocyanine green; OXP, oxaliplatin; PFP, perfluoropentane; I_NPs, ICG and PFP loaded nanoparticles; OI_NPs, ICG, PFP and OXP loaded nanoparticles; PSDT, photo-sonodynamic therapy; SD, standard deviation.

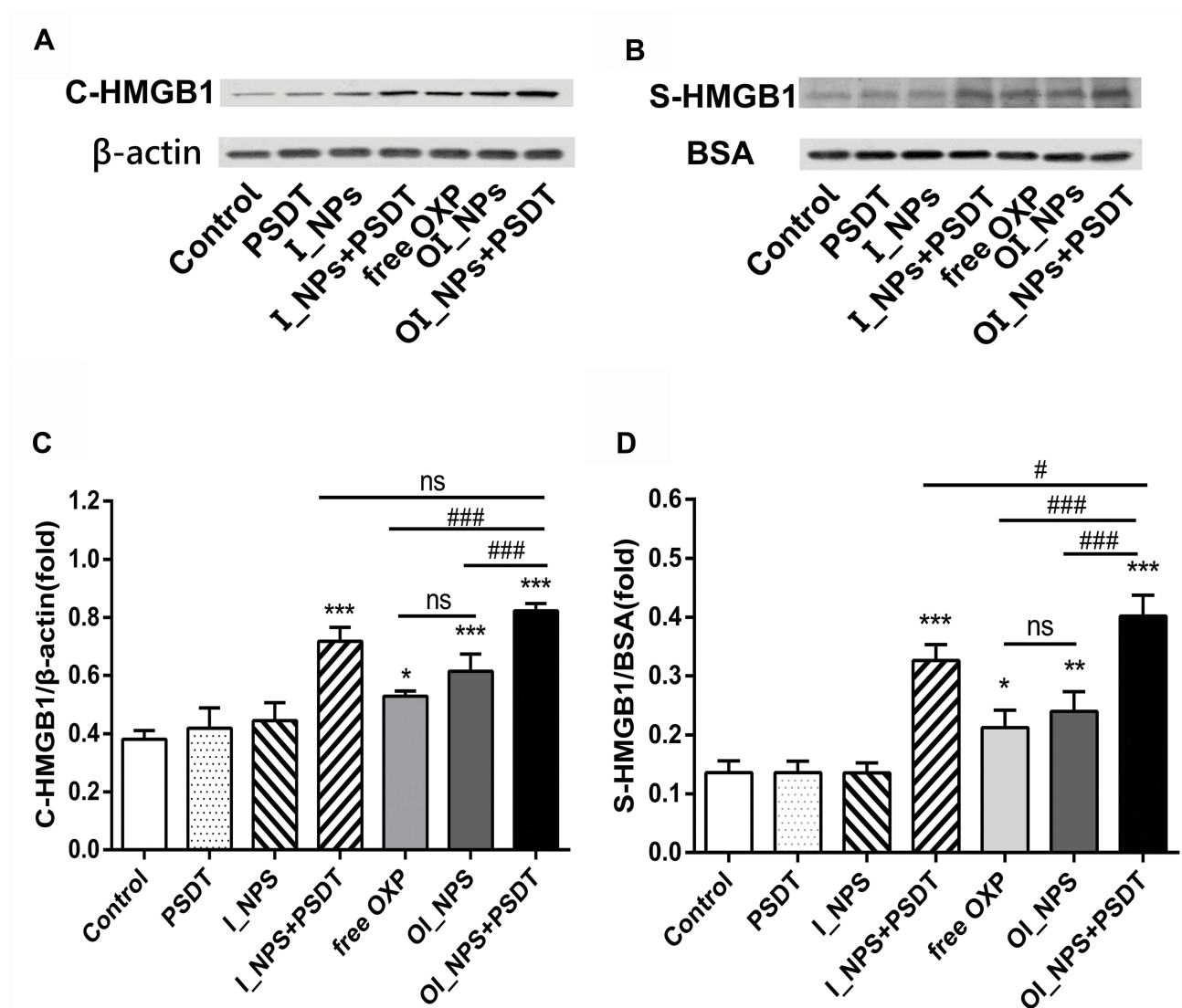


Figure 8 The release of HMGB1 in response to different treatments. (A) Cytosolic HMGB1 (C-HMGB1) was measured using Western blots; β -actin was used as a control. (B) The release of HMGB1 in the supernatant (S-HMGB1) was measured by Western blotting. BSA was used as the control protein. (C) Quantification of the band intensity of C-HMGB1 expression relative to β -actin. (D) Quantification of the band intensity of S-HMGB1 expression relative to BSA. Data in (C) and (D) are presented as means \pm SD (n=3). Data were analyzed by Student's t-tests and ANOVA. * $P < 0.05$, ** $P < 0.01$, *** $P < 0.001$ versus control group. # $P < 0.05$ and ### $P < 0.001$ between groups.

Abbreviations: HMGB1, high mobility group box 1; BSA, bovine serum albumin; ICG, indocyanine green; OXP, oxaliplatin; PFP, perfluoropentane; I_NPs, ICG and PFP loaded nanoparticles; OI_NPs, ICG, PFP and OXP loaded nanoparticles; PSDT, photo-sonodynamic therapy; SD, standard deviation; ns, no significant difference.

was used to analyze the translocation of HMGB1 to the cytoplasm, and its subsequent release into the supernatant of ID8 cells exposed to different treatments (Figure 8A and B). The translocation of HMGB1 to cytoplasm in OI_NPs+PSDT group was more than I_NPs+PSDT group, but there was no statistical difference between these two groups ($P > 0.05$) (Figure 8C). Cells treated with OI_NPs +PSDT produced the highest extent of HMGB1 release in supernatant than any of the other treatments (Figure 8D). Although the translocation and release of HMGB1 was more extensive in cells treated with OI_NPs compared to those treated with free OXP, there was no statistical difference between these two treatments (Figure 8C and D).

Intracellular ROS Generation And The Induction Of CRT

We used DCFH-DA as an indicator of ROS and used a combination of optical microscopy and a fluorescent microplate reader to observe and measure intracellular ROS production in ID8 cells in response to different treatments (Figure 9A and B). Previous studies have reported that the generation of ROS is important for ICD and that the capacity to induce ICD is associated with the production of ROS, although the mechanisms underlying these effects have not been elucidated.^{39,40} To determine the role of ROS in the PSDT modulation of CRT expression on the cell membrane, we

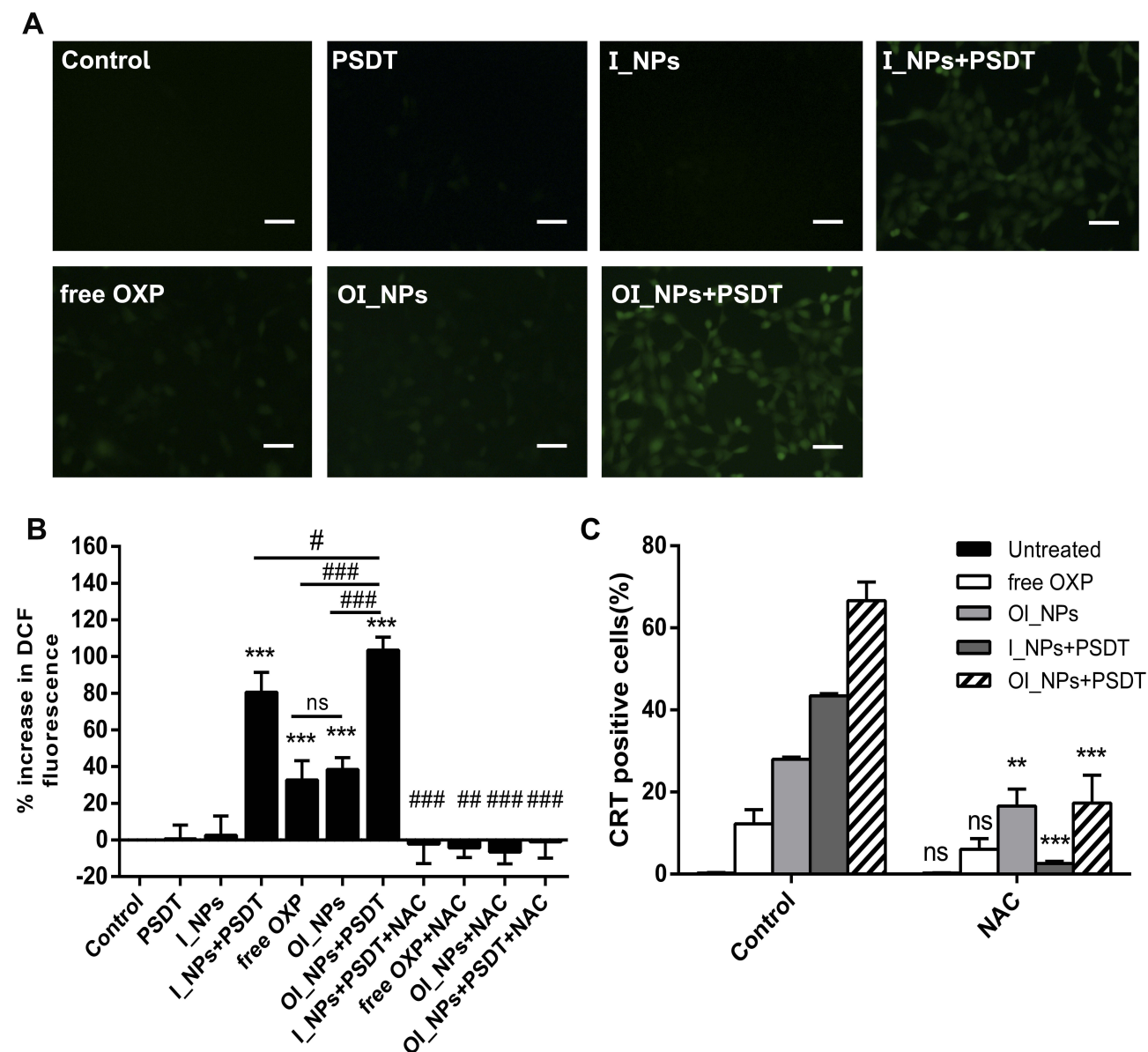


Figure 9 The determination of ROS production and the dependence of CRT on ROS. **(A)** The green fluorescent signal of DCF for the detection of ROS, as observed under fluorescence microscopy, scale bar represents 50 μ m. **(B)** ROS levels were measured using DCFH-DA. Fluorescence signals were detected with a fluorescence microplate reader. Data are shown as means \pm SD (n=3). Statistical analysis was performed using the Student's t-test and ANOVA. *** P <0.001 versus Control; # P <0.05, ### P <0.01, #### P <0.001 between groups. **(C)** A quantitative analysis of CRT surface exposure was performed by using flow cytometry to analyze ID8 cells with and without NAC prior to different treatments. (means \pm SD; n= 3 measurements; Student's t-test; ** P <0.01; *** P <0.001).

Abbreviations: CRT, calreticulin; ROS, reactive oxygen species; ICG, indocyanine green; OXP, oxalipatin; PFP, perfluoropentane; I_NPs, ICG and PFP loaded nanoparticles; OI_NPs, ICG, PFP and OXP loaded nanoparticles; PSDT, photo-sonodynamic therapy; DCF, 2',7'-dichlorofluorescein; DCFH-DA, 2',7'-dichlorofluorescein diacetate; NAC, N-acetylcysteine; ns, no significant difference.

compared the translocation of CRT to the cell surface in the presence or absence of N-Acetyl-L-cysteine (NAC), an inhibitor of ROS which scavenges ROS to scavenge cellular ROS. We found that the application of NAC completely inhibited the generation of intracellular ROS (Figure 9B) and that the expression of CRT was attenuated in all experimental groups but to varying extents (Figure 9C). In particular, the expression of CRT was dramatically attenuated in cells treated by I_NPs +

PSDT. These results illustrated that PSDT-induced ICD depends on the production of ROS.

Tumor Rechallenge And Cytotoxic T Lymphocyte Response

The gold standard for confirming the process of ICD in cancer cells is to inoculate immunocompetent mice with dying cancer cells that have been pre-treated with ICD

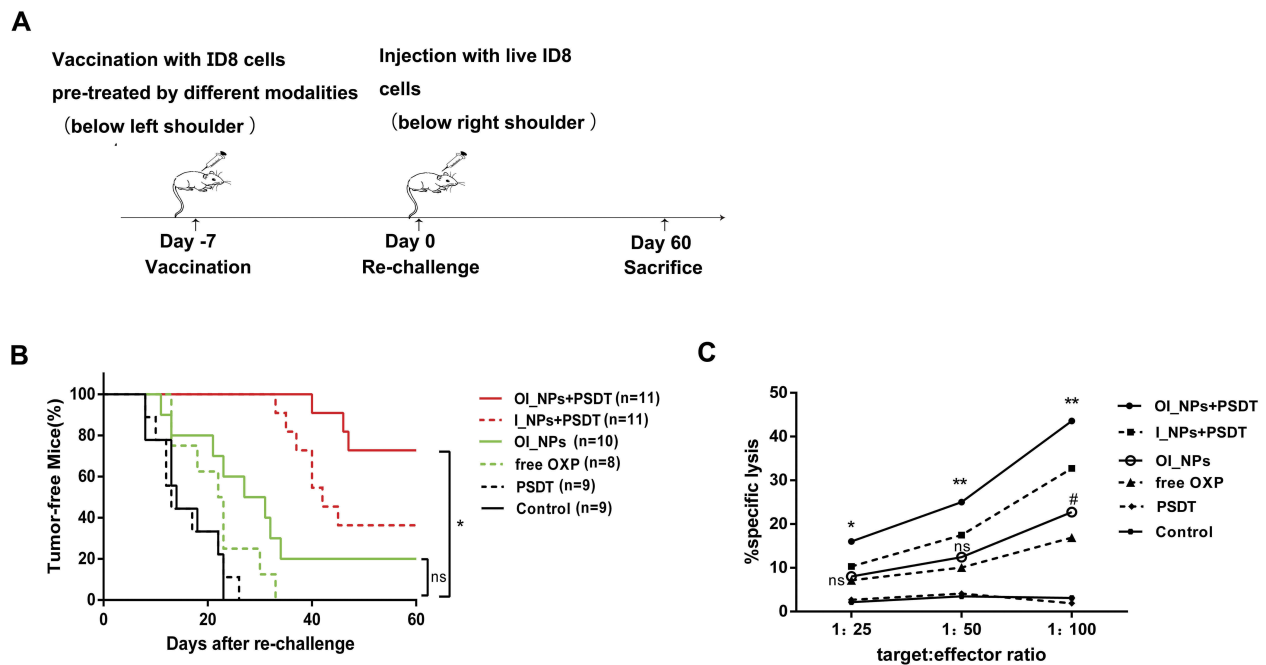


Figure 10 Tumor vaccination was effective against live tumor cells and specific CTL responses to ID8 cells. **(A)** Schematic illustration of the in vivo experiment used to evaluate the tumor vaccine potential of different modalities. ID8 cells, which had been treated in vitro with different treatments were inoculated subcutaneously into C57BL/6 mice. After 7 days, mice were rechallenged with live ID8 cells (syngeneic to the C57BL/6 mice). **(B)** The proportion of tumor-free mice is indicated. The Gehan-Breslow-Wilcoxon test was used for Kaplan Meier curves. * $P < 0.05$ versus the OI_NPs+PSDT group; ns denotes no significant difference. **(C)** Spleen cells isolated from vaccinated mice were collected as effector cells, and ID8 cells used as target tumor cells. Splenocytes and ID8 cells were co-incubated for 4h to detect CTL activity by using a lactate dehydrogenase releasing assay. Data in part C were carried out in triplicate, and the results are presented as means \pm SD ($n = 3$). Data were analyzed by ANOVA and Student's t -test. * $P < 0.05$ and ** $P < 0.01$ versus the OI_NPs+PSDT group. OI_NPs group versus free OXP group, # $P < 0.05$.

Abbreviations: ICG, indocyanine green; OXP, oxaliplatin; PFP, perfluoropentane; I_NPs, ICG and PFP loaded nanoparticles; OI_NPs, ICG, PFP and OXP loaded nanoparticles; PSDT, photo-sonodynamic therapy; CTL, Cytotoxic T lymphocyte; ns, no significant difference.

inducers in vitro against subsequent rechallenges with living cells of the identical origin.^{41,42} As shown in Figure 10A, pre-treated ID8 cells created in vitro as a tumor vaccine and then injected below the left shoulder of experimental mice. After 7 days later, the immunized mice were rechallenged by injecting live ID8 cells below the other shoulder. Our experiments showed that vaccination with control or PSDT-treated ID8 cells failed to elicit protection against the rechallenge (Figure 10B). Compared with control or PSDT-treated cells, those treated with free OXP showed a delay in the occurrence of tumors; however all mice ultimately lost any protective effect to reject ID8 cells at the tumor rechallenge site. The rate of inhibition for tumor occurrence of OI_NPs was higher than that obtained with free OXP, although this was not statistically significant. The inoculation of dying cancer cells pre-treated with I_NPs+PSDT, or OI_NPs + PSDT, significantly impeded tumor occurrence during the rechallenge experiments. Finally, the tumor free proportion of mice vaccinated with OI_NPs+PSDT was 72.73% ($P < 0.05$), thus indicating that this type of vaccination may have elicited a stronger immune response and thus delayed the

effects of the second inoculation. To assess the potency of vaccination on host T cell responses, we analyzed CTL activity (Figure 10C). In particular, we analyzed the proportion of cells undergoing lysis using ID8 cells as a target and after 4 h of incubation with splenocytes from mice that had been vaccinated with different formulations as an effector at multiple effector/target (E:T) ratios. The results showed that the OI_NPs+ PSDT treatment elicited stronger CTL activity and that this level of activity was significantly higher than that of the other treatments. T lymphocytes from the spleens of OI_NPs+ PSDT immunized mice were capable of lysing ID8 cells in an E/T-dependent pattern and showed the strongest ability to kill ID8 cells at E/T ratios of 100:1 ($P < 0.01$ versus other treatments). No statistical difference was observed between the OI_NPs and free OXP at 25:1 and 50:1 E/T ratio. When E/T ratio was at 100:1, there was significant statistical difference between these two groups ($P < 0.05$).

Discussion

Although traditional therapies have made noticeable improvements to the treatment of ovarian cancer, this

disease is still associated with high mortality rates in advanced stages and a high risk of recurrence.⁴³ Nevertheless, owing to the intricate features of ovarian malignancy, it is becoming evident that nanomedicine may provide very efficient treatment options.⁴⁴

In this study, we developed a nanoparticle modality that was combined with immunotherapy in an attempt to overcome the severe challenges imposed by tumors. We successfully entrapped the photo/sonosensitizer ICG, and the ICD inducer OXP, in PFP droplets using a double emulsion approach. Compared with free ICG, the entrapped ICG maintained steady optical absorption and fluorescence stability.

The combination of imaging and therapeutics for the diagnosis and treatment of tumors is receiving increasing levels of research attention. Liquid PFP droplets must be evaporated into gas bubbles in order to apply them as a valid US contrast agent; this is because their acoustic impedance values are analogous to that of the neighboring tissue.¹⁹ Following laser irradiation, the encapsulated ICG absorbs photons and creates an instantaneous increase in temperature, thus causing the PFP liquid droplets to vaporize to a gaseous phase for US imaging and PA signals. These attributes showed that our new NPs have the potential for a dual-model, imaging-guided, protocol for cancer treatment. In the future, we aim to apply our OI_NPs *in vivo* to investigate the therapeutic efficiency of these nanostructures and their ability to provide a dual-imaging model for tumor therapy.

The intracellular distribution and cellular uptake of important sensitizers plays a key role in the therapeutic effect of PDT and SDT.³⁷ The ability of ID8 cells to absorb OI_NPs was detected by CLSM and flow cytometry. Data clearly showed that the fluorescence intensity of cells incubated with OI_NPs was significantly enhanced, thus showing that OI_NPs can be internalized efficiently by ID8 cells. These data imply that our OI_NPs could be very beneficial for cancer therapy.

Twenty-four hours after a variety of different treatments, we used the MTT assay to determine cytotoxicity. Results showed that there was no significant cytotoxicity in cells treated by PSDT alone, indicating that the dose of light and ultrasound was not harmful to the ID8 cells. Furthermore, the OI_NPs+PSDT treatment option featured a combination of photodynamic, sonodynamic, and chemotherapeutic effects, and caused a greater inhibitory effect on cells than any of the other treatments. The results derived from our analysis of cell apoptosis under different therapeutic interventions were almost identical with data

produced by the MTT assays. Moreover, flow cytometry demonstrated that OI_NPs+PSDT showed a good level of anti-tumor efficacy when compared with other groups. OI_NPs encapsulating an equal concentration of OXP possessed a stronger ability to induce apoptosis than free OXP. It is probably the improved cellular uptake efficiency of NPs in comparison with free formulations and that this is a vital feature that increase their cytotoxicity.^{45,46}

Photo-sonodynamic therapy (PSDT), in combination with PDT and SDT, is an innovative and effective modality for the treatment of tumors. In previous studies, the application of PSDT was shown to reduce the amount of ultrasound/light energy required, and the dose of sensitizer, resulting in better antitumor efficacy than any form of monotherapy, and with fewer side effects.^{29,30,33} PFC PLGA nanoparticles may require a larger acoustic pressure in order to induce vaporization and collapse; this increase in pressure may cause damage to the surrounding healthy tissues during the percutaneous conversion of acoustic droplets. The application of a low-level laser to induce PFP vaporization is a vital first step; this augments the diameter of the OI_NPs and reduces the ultrasound power required for particle fragmentation. Simultaneously, this process eradicates impairment to the surrounding normal tissues. Hence, the efficiency of OI_NPs + PDT, and OI_NPs + SDT, were not tested because both laser and ultrasound treatment were considered to be indispensable interventions in our study for the evaporation and destruction of OI_NPs.

In order to confirm whether a combination therapy could induce ICD, and optimize the capacity for ICD induction, we selected three crucial ICD markers for evaluation. The expression of CRT, the secretion of ATP, and the release of HMGB1, in cells treated with OI_NPs+PSDT were all significantly higher than that of other groups. OI_NPs, when mediated by PSDT, exhibited important anti-tumor efficacy against ID8 cells, and showed significant potential to induce the exposure and release of tumor antigens for ICD induction. To confirm whether dying cancer cells undergo real ICD when treated with OI_NPs+PSDT, we rechallenged vaccinated C57BL/6 mice with living cells of the same origin. This successfully resulted in a protective effect against tumor rechallenge by OI_NPs-mediated PSDT and showed effective ability to induce ICD. Furthermore, LDH release experiments suggested that vaccination effects created by OI_NPs + PSDT could provoke T cell response and heighten cell-mediated immunoregulation to a greater extent than other treatments. Collectively, these findings

imply that OI_NPs+PSDT can serve as an effective inducer of real ICD and induce a greater release of DAMPs than other treatments. Although there was no statistical significance between OI_NPs and free OXP in terms of inducing the release of HMGB1, the OI_NPs resulted in a greater extent of CRT translocation and ATP secretion. Our results indicate that drug-loaded nanoparticles may enhance the capacity for ICD induction when compared to free formulations. Tumor vaccinations showed that both free OXP and OI_NPs delayed tumorigenesis after a second inoculation, and that the inhibitory rate in the OI_NPs treatment was higher than its free formulation; however, there was no statistical significance between the two modalities. This may have been because the concentration of OXP loaded into the OI_NPs was too low. Consequently, its ability to enhance the induction of ICD was restricted.

Several investigations have revealed that oxidative stress arising from the incremental generation of ROS is one of the major mechanisms involved in the induction of ICD.^{14,47} However, the precise mechanisms underlying between the production of intracellular ROS and the regulation of ICD is complicated and remains largely undetermined.^{39,40} In this study, we monitored the pivotal ICD signal, CRT, to explore the role of ROS in PSDT-induced ICD. We observed significant translocation of CRT in treatments producing large amounts of intracellular ROS. Furthermore, co-incubation with NAC significantly reduced the expression of CRT on ID8 cells, thus suggesting that a mechanism involving oxidative stress might play an indispensable role in regulating the ability of OXP and PSDT to induce CRT, particularly in terms of the response to PSDT. Impeding the generation of ROS could not completely eradicate the translocation of CRT in the free OXP and OI_NPs treatments, but may be involved with other, as yet unknown, mechanism. Further studies are now needed to elucidate the fundamental mechanisms underlying ROS-induced CRT exposure and optimize the formulation of our OI_NPs to gain the most effective antitumor immunity. PFC, as a highly effective oxygen carrier, can carry more oxygen compared with water or plasma.⁴⁸ With appropriate oxygenation, PFC may enhance the oxygen content of cells³⁶ and thus may improve their ability to induce ICD. Future studies should attempt to enhance the production of ROS in tumor therapies in order to induce ICD; this may improve the outcome of tumor immunotherapy.

The survival rates of ovarian cancer are associated with the number of immune cells infiltrating the tumor microenvironment, particularly T cells.^{49,50} The hallmarks of DAMPs, such as CRT, HMGB1, and ATP, are known to bind to their own

receptors on DCs. In turn, DCs are able to engulf tumor cells expressing antigens and present them such that they stimulate the activation and proliferation of T cells, particularly tumor-specific CD8⁺ T cells.⁵¹ OI_NPs with PSDT can combine ICD inducers. The work presented herein confirmed that this combination effectively enhanced the generation of vital DAMPs. However, we only explored the application of OI_NPs plus PSDT *in vitro*. Future work should investigate this modality *in vivo* to determine whether the release of tumor antigens into the tumor microenvironment will activate the infiltration of specific immune cells, such as T lymphocyte subsets. This process could eradicate tumors, improve survival rate and reduce the possibility of resistance.

Multifunctional OI_NPs have several advantages over other delivery systems. For example, these nanostructures are biodegradable, biocompatible, and exhibit high entrapment efficiency and optical stability, furthermore, combining imaging and therapeutic effects. These merits made OI_NPs can be as effective therapeutic delivery vehicles that could enhance the delivery of immunomodulatory materials, such as antibodies, cytokines, cancer vaccines, immunoadjuvant and adoptive cells. Such practice may result in significantly enhanced immunotherapeutic effects.

Some recent studies have utilized nanomedicine in combination with chemotherapeutic drugs and/or photodynamic therapy to induce ICD *in vitro*.^{52,53} More importantly, these therapies have applied immune checkpoint blockade therapy (PD-L1) and generated excellent anti-tumor immunity, not only eradicating the primary tumor but also significantly preventing metastatic tumors. Our treatment regimen can also be combined with immune checkpoint blockade therapy to augment immune and therapeutic effects. This combination may eliminate primary or metastatic neoplasm and evoke immunological memory to impede the recurrence of cancer and may allow its expansion to other aspects of tumor treatments.

Conclusion

In conclusion, we successfully fabricated OXP/ICG-loaded phase-transition nanoparticles (OI_NPs) using a double emulsion method. When combined with NIR laser and low-intensity ultrasound, OI_NPs can enhance both anti-tumor efficacy and immunogenic effects. Furthermore, owing to the excellent optical characteristics of ICG, and the phase-change ability of PFP, these novel NPs could serve as a dual-modality contrast agent for PA and US imaging. We believe that these OI_NPs have huge potential for cancer imaging and immunotherapy.

Acknowledgments

We would like to extend our thanks to Dr. Tinghe Yu (Director of the Key Medical laboratory of Obstetrics and Gynecology, The Second Affiliated Hospital, Chongqing Medical University, Chongqing, China) for support with regards to laboratory equipment. We would also like to thank Dr. Lan Hao (Institute of Ultrasound Imaging, The Second Hospital of Chongqing Medical University, Chongqing, China) for generous technical support. We are also grateful to Dr. Katherine Roby (University of Kansas Medical Center) and Dr. Yi Li (Peking University People's Hospital) for supplying the ID8 cells. This study was supported by the Natural Science Foundation of China (81972439, 81572558, 31630026), and the Natural Science Foundation of Chongqing (cstc2018jcyjAX0103, cstc2018jcyjAX0223).

Disclosure

None of the authors have any conflicts of interest to declare.

References

1. Srivastava SK, Ahmad A, Miree O, et al. Racial health disparities in ovarian cancer: not just black and white. *J Ovarian Res.* 2017;10(1):58. doi:10.1186/s13048-017-0355-y
2. Papaioannou NE, Beniata OV, Vitsos P, Tsitsilonis O, Samara P. Harnessing the immune system to improve cancer therapy. *Ann Transl Med.* 2016;4(14):261. doi:10.21037/atm.2016.04.01
3. Kroemer G, Galluzzi L, Kepp O, Zitvogel L. Immunogenic cell death in cancer therapy. *Annu Rev Immunol.* 2013;31:51–72. doi:10.1146/annurev-immunol-032712-100008
4. Krysko DV, Garg AD, Kaczmarek A, Krysko O, Agostinis P, Vandenabeele P. Immunogenic cell death and DAMPs in cancer therapy. *Nat Rev Cancer.* 2012;12(12):860–875. doi:10.1038/nrc3380
5. Panzarini E, Inguscio V, Dini L. Immunogenic cell death: can it be exploited in photodynamic therapy for cancer? *BioMed Res Int.* 2013;2013:482160. doi:10.1155/2013/482160
6. Chao MP, Jaiswal S, Weissman-Tsukamoto R, et al. Calreticulin is the dominant pro-phagocytic signal on multiple human cancers and is counterbalanced by CD47. *Sci Transl Med.* 2010;2(63):63ra94. doi:10.1126/scitranslmed.3001375
7. Gardai SJ, McPhillips KA, Frasch SC, et al. Cell-surface calreticulin initiates clearance of viable or apoptotic cells through trans-activation of LRP on the phagocyte. *Cell.* 2005;123(2):321–334. doi:10.1016/j.cell.2005.08.032
8. Apetoh L, Ghiringhelli F, Tesniere A, et al. Toll-like receptor 4-dependent contribution of the immune system to anticancer chemotherapy and radiotherapy. *Nat Med.* 2007;13(9):1050–1059. doi:10.1038/nm1622
9. Pisetsky DS, Gauley J, Ullal AJ. HMGB1 and microparticles as mediators of the immune response to cell death. *Antioxid Redox Signal.* 2011;15(8):2209–2219. doi:10.1089/ars.2010.3865
10. Elliott MR, Chekemi FB, Trampont PC, et al. Nucleotides released by apoptotic cells act as a find-me signal to promote phagocytic clearance. *Nature.* 2009;461(7261):282–286. doi:10.1038/nature08296
11. Ghiringhelli F, Apetoh L, Tesniere A, et al. Activation of the NLRP3 inflammasome in dendritic cells induces IL-1 β -dependent adaptive immunity against tumors. *Nat Med.* 2009;15(10):1170–1178. doi:10.1038/nm.2028
12. Adkins I, Fucikova J, Garg AD, Agostinis P, Spisek R. Physical modalities inducing immunogenic tumor cell death for cancer immunotherapy. *Oncoimmunology.* 2014;3(12):e968434. doi:10.4161/21624011.2014.968434
13. Tesniere A, Schlemmer F, Boige V, et al. Immunogenic death of colon cancer cells treated with oxaliplatin. *Oncogene.* 2010;29(4):482–491. doi:10.1038/onc.2009.356
14. Panaretakis T, Kepp O, Brockmeier U, et al. Mechanisms of pre-apoptotic calreticulin exposure in immunogenic cell death. *Embo J.* 2009;28(5):578–590. doi:10.1038/emboj.2009.1
15. Zhao X, Yang K, Zhao R, et al. Inducing enhanced immunogenic cell death with nanocarrier-based drug delivery systems for pancreatic cancer therapy. *Biomaterials.* 2016;102:187–197. doi:10.1016/j.biomaterials.2016.06.032
16. Liu WW, Liu SW, Liou YR, et al. Nanodroplet-vaporization-assisted sonoporation for highly effective delivery of photothermal treatment. *Sci Rep.* 2016;6:24753. doi:10.1038/srep24753
17. Sheng D, Liu T, Deng L, et al. Perfluorooctyl bromide & indocyanine green co-loaded nanoliposomes for enhanced multimodal imaging-guided phototherapy. *Biomaterials.* 2018;165:1–13. doi:10.1016/j.biomaterials.2018.02.041
18. Deng L, Cai X, Sheng D, et al. A laser-activated biocompatible theranostic nanoagent for targeted multimodal imaging and photothermal therapy. *Theranostics.* 2017;7(18):4410–4423. doi:10.7150/thno.21283
19. Strohm E, Rui M, Gorelikov I, Matsuura N, Kolios M. Vaporization of perfluorocarbon droplets using optical irradiation. *Biomed Opt Express.* 2011;2(6):1432–1442. doi:10.1364/BOE.2.001432
20. Niu C, Wang L, Wang Z, Xu Y, Hu Y, Peng Q. Laser irradiated fluorescent perfluorocarbon microparticles in 2-D and 3-D breast cancer cell models. *Sci Rep.* 2017;7:43408. doi:10.1038/srep43408
21. Li B, Lin L, Lin H, Wilson BC. Photosensitized singlet oxygen generation and detection: recent advances and future perspectives in cancer photodynamic therapy. *J Biophotonics.* 2016;9(11–12):1314–1325. doi:10.1002/jbio.201600055
22. Dąbrowski JM. Reactive oxygen species in photodynamic therapy: mechanisms of their generation and potentiation. *Adv Inorg Chem.* 2017;70:343–394.
23. Garg AD, Krysko DV, Verfaillie T, et al. A novel pathway combining calreticulin exposure and ATP secretion in immunogenic cancer cell death. *Embo J.* 2012;31(5):1062–1079. doi:10.1038/emboj.2011.497
24. Garg AD, Vandenberk L, Koks C, et al. Dendritic cell vaccines based on immunogenic cell death elicit danger signals and T cell-driven rejection of high-grade glioma. *Sci Transl Med.* 2016;8(328):328ra327. doi:10.1126/scitranslmed.aae0105
25. Liang R, Liu L, He H, et al. Oxygen-boosted immunogenic photodynamic therapy with gold nanocages@manganese dioxide to inhibit tumor growth and metastases. *Biomaterials.* 2018;177:149–160. doi:10.1016/j.biomaterials.2018.05.051
26. Zhang JY, Chen S, Wang P, et al. NaYbF₄ nanoparticles as near infrared light excited inorganic photosensitizers for deep penetration in photodynamic therapy. *Nanoscale.* 2017;9(8):2706–2710. doi:10.1039/C6NR09401E
27. Chen YW, Liu TY, Chang PH, et al. A theranostic nrGO@MSN-ION nanocarrier developed to enhance the combination effect of sonodynamic therapy and ultrasound hyperthermia for treating tumor. *Nanoscale.* 2016;8(25):12648–12657. doi:10.1039/C5NR07782F
28. Qian X, Zheng Y, Chen Y. Micro/nanoparticle-augmented Sonodynamic Therapy (SDT): breaking the depth shallow of photoactivation. *Adv Mater.* 2016;28(37):8097–8129. doi:10.1002/adma.201602012
29. Liu Y, Wang P, Liu Q, Wang X. Sinoporphyrin sodium triggered sono-photodynamic effects on breast cancer both in vitro and in vivo. *Ultrason Sonochem.* 2016;31:437–448. doi:10.1016/j.ultsonch.2016.01.038

30. Wang P, Li C, Wang X, et al. Anti-metastatic and pro-apoptotic effects elicited by combination photodynamic therapy with sonodynamic therapy on breast cancer both in vitro and in vivo. *Ultrason Sonochem.* 2015;23:116–127. doi:10.1016/j.ulsonch.2014.10.027
31. Chen HJ, Zhou XB, Wang AL, Zheng BY, Yeh CK, Huang JD. Synthesis and biological characterization of novel rose bengal derivatives with improved amphiphilicity for sono-photodynamic therapy. *Eur J Med Chem.* 2018;145:86–95. doi:10.1016/j.ejmech.2017.12.091
32. Zhang Q, Bao C, Cai X, et al. Sonodynamic therapy-assisted immunotherapy: a novel modality for cancer treatment. *Cancer Sci.* 2018;109(5):1330–1345. doi:10.1111/cas.13578
33. Wang H, Wang X, Wang P, Zhang K, Yang S, Liu Q. Ultrasound enhances the efficacy of chlorin E6-mediated photodynamic therapy in MDA-MB-231 cells. *Ultrasound Med Biol.* 2013;39(9):1713–1724. doi:10.1016/j.ultrasmedbio.2013.03.017
34. Porcu EP, Salis A, Gavini E, Rassa G, Maestri M, Giunchedi P. Indocyanine green delivery systems for tumour detection and treatments. *Biotechnol Adv.* 2016;34(5):768–789. doi:10.1016/j.biotechadv.2016.04.001
35. Nomikou N, Sterrett C, Arthur C, McCaughan B, Callan JF, McHale AP. The effects of ultrasound and light on indocyanine-green-treated tumour cells and tissues. *ChemMedChem.* 2012;7(8):1465–1471. doi:10.1002/cmdc.201200233
36. Chen S, Liu Y, Zhu S, et al. Dual-mode imaging and therapeutic effects of drug-loaded phase-transition nanoparticles combined with near-infrared laser and low-intensity ultrasound on ovarian cancer. *Drug Deliv.* 2018;25(1):1683–1693. doi:10.1080/10717544.2018.1507062
37. Tang Q, Cui J, Tian Z, et al. Oxygen and indocyanine green loaded phase-transition nanoparticle-mediated photo-sonodynamic cytotoxic effects on rheumatoid arthritis fibroblast-like synoviocytes. *Int J Nanomed.* 2017;12:381–393. doi:10.2147/IJN.S120902
38. Castano AP, Mroz P, Wu MX, Hamblin MR. Photodynamic therapy plus low-dose cyclophosphamide generates antitumor immunity in a mouse model. *Proc Natl Acad Sci U S A.* 2008;105(14):5495–5500. doi:10.1073/pnas.0709256105
39. Zitvogel L, Kepp O, Senovilla L, Menger L, Chaput N, Kroemer G. Immunogenic tumor cell death for optimal anticancer therapy: the calreticulin exposure pathway. *Clin Cancer Res.* 2010;16(12):3100–3104. doi:10.1158/1078-0432.CCR-09-2891
40. Sun C, Wang H, Mao S, Liu J, Li S, Wang J. Reactive oxygen species involved in CT26 immunogenic cell death induced by Clostridium difficile toxin B. *Immunol Lett.* 2015;164(2):65–71. doi:10.1016/j.imlet.2015.02.007
41. Casares N, Pequignot MO, Tesniere A, et al. Caspase-dependent immunogenicity of doxorubicin-induced tumor cell death. *J Exp Med.* 2005;202(12):1691–1701. doi:10.1084/jem.20050915
42. Obeid M, Tesniere A, Panaretakis T, et al. Ecto-calreticulin in immunogenic chemotherapy. *Immunol Rev.* 2007;220:22–34. doi:10.1111/j.1600-065X.2007.00567.x
43. Kim HS, Han HD, Armaiz-Pena GN, et al. Functional roles of Src and Fgr in ovarian carcinoma. *Clin Cancer Res.* 2011;17(7):1713–1721. doi:10.1158/1078-0432.CCR-10-2081
44. Mir Y, Elrington SA, Hasan T. A new nanoconstruct for epidermal growth factor receptor-targeted photo-immunotherapy of ovarian cancer. *Nanomedicine.* 2013;9(7):1114–1122. doi:10.1016/j.nano.2013.02.005
45. Vivek R, Thangam R, Nipunbabu V, Ponraj T, Kannan S. Oxaliplatin-chitosan nanoparticles induced intrinsic apoptotic signaling pathway: a “smart” drug delivery system to breast cancer cell therapy. *Int J Biol Macromol.* 2014;65:289–297. doi:10.1016/j.ijbiomac.2014.01.054
46. Brown SD, Nativo P, Smith JA, et al. Gold nanoparticles for the improved anticancer drug delivery of the active component of oxaliplatin. *J Am Chem Soc.* 2010;132(13):4678–4684. doi:10.1021/ja908117a
47. Lin A, Truong B, Patel S, et al. Nanosecond-pulsed DBD plasma-generated reactive oxygen species trigger immunogenic cell death in A549 lung carcinoma cells through intracellular oxidative stress. *Int J Mol Sci.* 2017;18(5). doi:10.3390/ijms18050966
48. Riess JG. Perfluorocarbon-based oxygen delivery. *Artif Cells Blood Substit Immobil Biotechnol.* 2006;34(6):567. doi:10.1080/10731190600973824
49. Zhang L, Conejo-Garcia JR, Katsaros D, et al. Intratumoral T cells, recurrence, and survival in epithelial ovarian cancer. *N Engl J Med.* 2003;348(3):203–213. doi:10.1056/NEJMoa020177
50. Mandai M, Hamanishi J, Abiko K, Matsumura N, Baba T, Konishi I. Anti-PD-L1/PD-1 immune therapies in ovarian cancer: basic mechanism and future clinical application. *Int J Clin Oncol.* 2016;21(3):456–461. doi:10.1007/s10147-016-0968-y
51. Green DR, Ferguson T, Zitvogel L, Kroemer G. Immunogenic and tolerogenic cell death. *Nat Rev Immunol.* 2009;9(5):353–363. doi:10.1038/nri2545
52. Duan X, Chan C, Guo N, Han W, Weichselbaum RR, Lin W. Photodynamic therapy mediated by nontoxic core-shell nanoparticles synergizes with immune checkpoint blockade to elicit antitumor immunity and antimetastatic effect on breast cancer. *J Am Chem Soc.* 2016;138(51):16686–16695. doi:10.1021/jacs.6b09538
53. He C, Duan X, Guo N, et al. Core-shell nanoscale coordination polymers combine chemotherapy and photodynamic therapy to potentiate checkpoint blockade cancer immunotherapy. *Nat Commun.* 2016;7:12499. doi:10.1038/ncomms12499

International Journal of Nanomedicine

Publish your work in this journal

The International Journal of Nanomedicine is an international, peer-reviewed journal focusing on the application of nanotechnology in diagnostics, therapeutics, and drug delivery systems throughout the biomedical field. This journal is indexed on PubMed Central, MedLine, CAS, SciSearch®, Current Contents®/Clinical Medicine,

Submit your manuscript here: <https://www.dovepress.com/international-journal-of-nanomedicine-journal>

Dovepress

Journal Citation Reports/Science Edition, EMBASE, Scopus and the Elsevier Bibliographic databases. The manuscript management system is completely online and includes a very quick and fair peer-review system, which is all easy to use. Visit <http://www.dovepress.com/testimonials.php> to read real quotes from published authors.